Interactions of amphipathic α-helical MEG proteins from *Schistosoma mansoni* with membranes

Ana P Felizatti[1], Ana E Zeraik[1], Luis GM Basso[2], Patricia S Kumagai[1], Jose LS Lopes[3], BA Wallace[4], Ana PU Araujo[1], Ricardo DeMarco[1]

[1] Instituto de Física de São Carlos, Universidade de São Paulo, Av João Dagnone 1100, São Carlos, SP 13563-120, Brasil

[2] Faculdade de Filosofia, Ciências e Letras de Ribeirão Preto, Universidade de São Paulo, Av. Bandeirantes 3900, Ribeirão Preto, SP 14040-901, Brasil

[3] Instituto de Física, Universidade de São Paulo, Rua do Matão 1371, São Paulo, SP 05508-090, Brasil

[4] Institute of Structural and Molecular Biology, Birkbeck College, University of London, Malet St, London, WC1E 7HX, UK

* Corresponding author: Prof. Dr. Ricardo DeMarco

Depto. Física e Ciências Interdisciplinares, Instituto de Física de São Carlos, USP

Av. João Dagnone 1100, 13563-120, São Carlos, SP, Brasil

Phone: +55(16)

rdemarco@ifsc.usp.br

Abstract

Micro Exon Gene (MEG) proteins are thought to play major roles in the infection and survival of parasitic *Schistosoma mansoni* worms in host organisms. Here, the physical chemical properties of two small MEG proteins found in the genome of *S. mansoni*, named MEG-24 and MEG-27, were examined by a combination of biophysical techniques such as differential scanning calorimetry, tensiometry, circular dichroism, fluorescence, and electron spin resonance spectroscopies. The proteins are surface active and structurally arranged as cationic amphipathic α-helices that can associate with lipid membranes and cause their disruption. After adsorption to lipid membranes, MEG-27 strongly affects the fluidity of erythrocyte ghost membranes, whereas MEG-24 forms pores in erythrocytes without modifying the ghost membrane fluidity. Whole–mount in situ hybridization experiments indicates that MEG-27 and MEG-24 transcripts are located in the parasite esophagus and tegument, respectively, suggesting a relevant role of these proteins in the host-parasite interface. Taken together, these characteristics lead us to propose that these MEG proteins may interact with host cell membranes and potentially modulate the immune process using a similar mechanism as that described for α-helical membrane active peptides.

Keywords: micron-exon gene proteins, *Schistosoma mansoni*, circular dichroism spectroscopy; mechanism of action; peptide-lipid interactions.

Abbreviations: MEG, micro exon gene; SUVs, small unilamellar vesicles; LUVs, large unilamellar vesicles; DSC, differential scanning calorimetry; OCD, SRCD, synchrotron radiation circular dichroism; ESR, electron spin resonance.

1. Introduction

Schistosomiasis is a widely spread tropical disease caused by organisms of the *Schistosoma* genera, with *Schistosoma mansoni* as one of the main causative agents, being prevalent in tropical regions of Africa and the Americas [1,2] The analysis of *S. mansoni* genome revealed an intriguing class of genes consisting of small (<36 bp) and symmetric exons, which have been designated as Micro Exon Genes (MEGs) [3,4]. These genes encode small proteins, ranging from 6 to 20 kDa, which have been suggested to play important roles in the host-parasite interface [4]: Their expression is concentrated in intramammalian stages and in the esophagus and tegument, which are tissues of the parasite in direct contact with host cells.

The sequences of MEG proteins include predicted signal peptides, suggesting targeting to extracellular membranes. Several MEG proteins have been detected by proteomics in parasite secretions or tegument surfaces [4], thus confirming their exposure to the host membranes. MEGs display an accelerated evolution, with nonsynonymous/synonymous substitution rates (dN/dS) higher than most vaccine candidates and an expansion in gene copy numbers, indicating an intense evolutionary pressure from the host immune system [5]. The fact that MEGs display small symmetrical exons allows for the generation of multiple alternatively-spliced transcripts that code for proteins with small changes in their sequences [4,5]. This ability appears to be the basis of their mechanism of antigenic variation, which allows the detection of multiple proteins with different molecular weights and pIs derived from the same gene.

Orthologs of *S. mansoni* MEGs have been detected only in other organisms of the *Schistosoma* genera and in the *Trichobilharzia regenti* [6]. Therefore, the function of MEGs cannot be attributed based on homology with proteins with known function or conserved domains. Protein structure predictions of MEGs suggest that polipeptides coded by several

MEG families include a large portion of disordered structure. This was experimentally confirmed for MEG-14, which has been classified as an intrinsically disordered protein [7,8]. However, several other MEG families have also been predicted to be mainly composed of α-helix structure with an amphipathic nature [9]

Evidence of MEG proteins interacting with cells from the immune system has been obtained by immunofluorescence microscopy of MEG-4, which showed staining of a halo surrounding ingested leukocytes [10] and high concentrations of MEG-4 in the parasite esophagus. These results have led to the proposal that the MEG proteins might act as important players in blood processing [6,9]. In addition, yeast two-hybrid system, pull down and surface plasmon resonance experiments showed that the protein MEG-14 [7] interacts with the human S100A9, a protein involved in inflammatory signaling process and highly expressed in some cells of the immune system [8]

In this study, we perform the characterization of two novel small *Schistosoma mansoni* MEG proteins (MEG-24 and MEG-27) that are expressed at different sites in adult worms. Both MEGs are arranged in amphipathic helices and interact with membrane models and cell membranes, however using different mechanisms. Similar to what is observed for the membrane active peptides [11–13], which are naturally-occurring compounds that interact with the cell membrane (either passing through it, or inserting at the membrane interface, or even causing its disruption), it is believed that specific interactions of these small MEG proteins with cell membranes may also disturb the lipid layer physical integrity.

Great interest has been placed in molecules that act modulating the human immune response. The functions related to this modulation include direct chemotactic activity towards leukocytes, regulation of TLR-dependent inflammatory responses and promotion of wound healing [14,15]

Despite both proteins displayed membranolytic function on model membranes, only MEG-24 has shown pore-forming properties on more complex cell membranes such as those from red blood cells. However, MEG-27 also interacts with erythrocyte ghost membranes, changing the lipid bilayer fluidity and the melting profiles of the ghost membrane proteins. Thus, we hypothesize that MEGs may interact with host cells and putatively influence the host immune response system.

2. Experimental section

2.1. Peptide design and sequence analysis

As MEG-24 and MEG-27 are both small protein, two polipeptides were designed based on the predicted sequence of the mature MEG proteins (signalP program was used to exclude the signal peptide), thus MEG-24 (AAVILHPKYEMTFTEKLRFYFRCLVKVLC HMIRLGYIGPLSDYYVH) and MEG-27 (IKWVNCSHELNEHTSETSLRRWIHTVFSFL FHNF) were custom synthesized by Genscript, EUA. Predictions of secondary structure were performed by PSIPRED Server software (http://bioinf.cs.ucl.ac.uk/psipred/). The hydrophobicity analysis was performed with the HELIQUEST software (http://heliquest.ipmc.cnrs.fr/cgi-bin/ComputParamsV2.py). Prediction of transmembrane regions was carried out using Phobius [16] [and TMHMM [17]

2.2. Whole mount in situ hybridization (WISH)

To assess mRNA expression sites of the MEGs, WISH experiments were performed according to a previously described WISH protocol optimized for schistosomes [18]. MEG-24 and MEG-27 antisense RNAs were used as probes and sense RNA strand as the control.

2.3. Liposome preparation

Lipid vesicles were prepared with POPC (1-palmitoyl-2-oleoyl-sn-glycero-3-phosphocholine), POPG (1-palmitoyl-2-oleoyl-sn-glycero-3-phospho-(1'-rac-glycerol), POPE (1-palmitoyl-2-oleoyl-sn-glycero-3-phosphoethanolamine), cholesterol, sphingomyelin (N-octadecanoyl-D-erythrosphingosylphosphorylcholine), and DMPC (1,2-dimyristoyl-sn-glycero-3-phosphocholine). All lipids were purchased from Avanti Polar Lipids. Phospholipids (5 mg/mL) solubilized in chloroform/methanol mixture 4:1 (v/v) were deposited in glass tubes and the solvent was slowly evaporated under a continuous nitrogen flow, resulting in the formation of a lipid film. An additional drying step was performed using a SpeedVac ™ concentrator (SAVANT ™) for at least 4 h. Subsequently, the film was resuspended in an appropriate buffer (as specified in each section) for 16 h at 42 ^{o}C. The resulting multilamellar vesicles were then subjected to 10 cycles of freezing and thawing. Small unilamellar vesicles (SUVs) were prepared by submitting the freeze-thawed lipid sample to probe tip sonication (5 cycles of 50 seconds) at room temperature. Large unilamellar vesicles (LUVs) loaded with 35 mM calcein in water were prepared by submitting the freeze-thawed vesicles to an extruder with 0.2 μm polycarbonate membrane to select vesicles with standardized radii. After extrusion, the sample was loaded on a Sephadex G-50 (Sigma Aldrich) 20 cm x 1 cm column to remove the nonencapsulated calcein from the dye-trapped LUVs. After elution, the liposome concentration was determined using an organic phosphorous assay [19]

2.5. Intrinsic tryptophan emission spectrum and calcein leakage (CL) assays

The emission spectra of the Trp residues of MEG-27 in ultrapure water and in the presence of SUVs of POPC (at a 1:100 peptide-to-lipid molar ratio) were measured at 25 ^{o}C in a K2 Fluorometer (ISS-IL), with a 1-cm pathlength quartz cell and magnetic stirring. The sample was excited at 295 nm and the emission spectrum was monitored from 300 to 500 nm.

The effects of MEG-24 and MEG-27 on membrane permeability were studied by measuring the leakage of the fluorescent dye from calcein-entrapped liposomes in 10 mM HEPES buffer pH 7.4, 100 mM NaCl. Different peptide-to-lipid molar ratios (1:20, 1:50, 1:100, 1:250, 1:500, 1:1000 and 1:5000) were used and the kinetics was monitored for 600 seconds, with the excitation wavelength set to 495 nm and the emission monitored at 520 nm. As control of total lysis, liposomes were solubilized with 1% Triton X-100 after each measurement.

2.6. Differential scanning calorimetry (DSC)

LUVs of DMPC in Phosphate-buffered saline were incubated with MEG proteins for 30 min at 37 ºC at diferent lipid-to-peptide molar ratios. DSC measurements were carried out using a heating rate of 30 ºC/h and a temperature range of 6 to 45 ºC. The equilibration period was 15 minutes at 6 ºC. Erythrocyte ghost membranes were prepared as described in [20]. Aliquots were prepared and stored refrigerated until use for up to three days. For reference scan, 300 mg/ml of ghost in PBS solution were used. For proteins analisys, 100 mg/ml of ghost in PBS solution were incubated with the peptides at 37 °C for 20 min prior to the experiments. The peptide concentrations were 1 µM, 5 µM and 15 µM. The heating rate was 60 ºC/h and the temperature range of 15 to 90 ºC. The equilibration period was 10 minutes at 15 ºC. All experiments were performed using a microcalorimeter VP-DSC (MicroCal). The analysis of thermograms was carried out using MicroCal software, developed within the software Origin 7.0.

2.7. Electron spin resonance (ESR) spectroscopy

ESR experiments were carried out on an X-band E-109 Varian ESR spectrometer using the following acquisition parameters: field modulation frequency, 100 kHz; field

modulation amplitude, 0.5 or 1.0 G; microwave power, 5 mW; and scan width, 100 to 160 G. Erythrocyte ghost membranes for ESR were prepared as follows: An erythrocyte ghost solution was centrifuged at 15,000 × g and the pellet dried at 37 °C for 1 h. The dry ghost mass was weighed and divided into 100 mg aliquots, which were resuspended in 1 mL of hypotonic buffer (5 mM KCl, 5mM Tris-HCl, pH 7.4) in the presence of 100 µL of nitroxide-labeled lipids at 1 mg/mL. The mixture was incubated for 1 hour at 37 ºC. Then, the ghosts were centrifuged at 1,500 × g for 1 min and the supernatant was replaced with 1 mL of fresh PBS. This washing procedure was repeated 4 times to remove excess spin label. After the final wash, the pellet (100 mg) was resuspended in 100 uL of PBS. Three nitroxide lipid probes, purchased from Avanti Polar Lipids, Inc. (Alabaster, AL), were used: 1,2-dipalmitoyl-sn-glycero-3-phospho(tempo)choline (DPPTC), for monitoring the polar region (surface); and 1-palmitoyl-2-stearoyl(n-doxyl)-sn-glycero-3-phosphocholine (n-PCSL, where n = 5 and 16), to monitor the hydrophobic region of the lipid bilayer. POPC/spin labels SUVs samples for ESR were prepared as described in section 2.3 with the only modification that both lipid and spin labels solubilized in organic solvent were mixed in a glass tube. The samples were inserted into capillaries that were sealed and centrifuged prior to the measurements.

Nonlinear least-squares simulations (NLLS) of the ESR spectra were carried out as previously described [21]using the Multicomponent LabView (National Instruments) software (http://www.biochemistry.ucla.edu/Faculty/Hubbell/). The components of the g- and hyperfine tensors used in the NLLS simulations are shown in Table S1.

2.8. Circular dichroism (CD) spectroscopy

Conventional CD measurements were performed at 25 °C on a Jasco J-815 spectrometer using a quartz cuvette with a 1 mm pathlength. Eight consecutive scans at scanning speed of 50 nm/min, bandwidth of 1 nm and response of 1s were averaged for each condition over the

wavelength range of 270 to 195 nm, in 1 nm intervals. MEG-24 or MEG-27 (15 μM) were solubilized in water, in the presence or absence of POPC vesicles at different lipid-to-peptide molar ratios. The synchrotron radiation circular dichroism (SRCD) spectra of the MEG proteins in aqueous solution and in the presene of POPC vesicles were obtained at the AU-CD beamline on the ASTRID2 synchrotron (Aarhus University, Denmark). The spectra were obtained at 25 ºC with the measurement of 3 scans over the wavelength range from 280 to 170 nm, with bandwidth of 1 nm and 2 s dwell time, using a demountable quartz Suprasil cuvette (Hellma Analytics, UK) with a 0.0097 cm pathlength. All CD/SRCD spectra were processed using the CDtool [22] software, which consisted of averaging the scans collected, subtracting the respective baseline spectrum, zeroing in the 263–270 nm region, and smoothing with a Savitzky–Golay filter. The DichroWeb analysis server [23] was used to calculate the secondary structure content using the CDSSTR method and the reference data set SP175 [24] The goodness of the fit was evaluated by the calculation of the normalized root mean-square deviation (NRMSD) for each analysis [25]

Oriented lipid bilayers were prepared with the cosolubilization of POPC and the MEG proteins in a mixture of chloroform/methanol 4:1 (v/v) at 1:50 peptide-to-lipid molar ratio, followed by the deposition of the mixture onto a circular quartz glass Suprasil plate (Hellma Analytics, UK). The plates were dried in a desiccator under vacuum for 3 h to evaporate the solvent, and then rehydrated for 16 h in sealed chambers with a saturated solution of K_2SO_4. The oriented CD (OCD) spectra were obtained using a Jasco J-720 CD instrument from 280 to 190 nm, taking 4 different rotational positions of the plate (0, 90, 180, and 270 degrees), which was arranged perpendicular to the light beam. The spectra of the lipids alone were subtracted from the final spectrum.

2.9. Surface tension measurements and adsorption on Langmuir monolayers

The surface activity of MEG-24 and MEG-27 in aqueous solution was assayed in a Delta Pi Langmuir-tensiometer (Kibron, Finland) taking measurements for 4 h, at 25^{o}C, with MEG-24 and MEG-27 at 10 μM in pure MilliQ water. In addition, small amounts of POPC solubilized in methanol/hexane (10/1, v/v, at a 1 mg/mL) were spread on the air/water interface of a microplate well filled with 1.2 mL MilliQ water, to generate lipid monolayers with lateral packing density of 15, 25 and 35 mN/m. Subsequently, each MEG protein (10 μM) was injected to the aqueous subphase and the adsorption kinetics of the proteins on Langmuir monolayers of POPC were monitored until reaching equilibrium (~2 h).

2.10. Hemolytic assay

The protocol for blood collection was approved by a research ethics committee from Universidade Federal de São Carlos (protocol number 823.540). Informed consent was obtained from a healthy volunteer human donor. The collected blood (1 mL) was diluted 10× (v/v) in PBS (pH 7.4), then centrifuged at 3500 × g for 10 min at 4 ^{o}C to separate the red blood cells. Cycles of centrifugation followed by removal of the supernatant were performed until the aqueous solution remained clear and colourless after centrifugation. A 1% solution of the red cell pellet was then diluted in PBS and aliquoted (100 μL) into 96-well microplates. Controls (negative, water, positive, Triton 1% solution) and the MEG proteins at concentrations ranging from 0.5 μM to 5 μM were added in duplicate. The plate was incubated at 37 °C for 1 h. Hemoglobin was detected in the supernatant at 409 nm in a spectrophotometer coupled to a SpectraMaxi3x microplate reader (Molecular Devices).

2.11. Osmotic protection and pore-size estimation

The method utilized for osmotic protection and pore size estimation was based on a previously described protocol [26]. Briefly, PEGs of different radii were used as osmotic

protectors to determine the average pore size formed in the membrane induced by the proteins. The following PEGs of known hydrated diameters were used [26, 27]: PEG 200 (~ 0.9 nm), PEG 300 (~ 1.2 nm), PEG 400 (~ 1.4 nm), PEG 600 (~ 1.5 nm), PEG 900 (~ 1.7 nm), PEG 1000 (~ 1.8 nm), PEG 1500 (~ 2.4 nm), PEG 3000 (~ 3.0 nm), and PEG 6000 (~ 5 nm). 100 µl aliquots of a 1% red blood cell suspension were added to 100 µl of a 30 mM PEG solution in PBS, pH 7.4, and then incubated with 80 µM of MEG-24 for 1 h at 37 ºC. The amount of hemoglobin released in the supernatant was measured in a plate reader at 409 nm wavelength.

3. Results

3.1. Amphipatic helical MEGs are expressed both in the adult worm esophagus and tegument

Bioinformatics studies performed with MEG-24 and MEG-27 sequences reveal that both peptides are predicted to have secondary structure mainly composed of α-helical elements (Figure S1A). The helical wheel projections of the predicted helices in MEG-24 and MEG-27 clearly show their amphipathic character, displaying two opposing hydrophilic and hydrophobic faces (Figure S1B). Both sequences exhibit a net positive charge in the hydrophilic face of +2 for MEG-27, and +5 for MEG-24, which characterize these proteins as cationic amphipathic helices. The distribution of the amino acid residues along the peptides primary structure is quite different, though. While MEG-24 displays the apolar and the acid/basic residues regularly distributed along the peptide sequence, MEG-27 exhibits a polarity gradient, with a more hydrophilic N-terminal segment and a more hydrophobic C-terminus (Figure S1C). Searches for transmembrane regions in the MEG proteins using Phobius and TMHMM indicate that only MEG-24 sequence is predicted to adopt a

transmembrane topology, most likely between residues 19 and 41, if we only consider residues with probability of belonging to a transmembrane domain above 0.1 (Figure S1D).

The existence of MEGs displaying an amphipathic structure similar to that found in α-helical membrane-active peptides [27] may suggest a possible analogous function for these peptides. Data from RNA-Seq showed an enrichment of MEG-27 transcripts in schistosome heads, thus suggesting a focal expression in the esophagus [9]. Such a trend is absent for transcripts from MEG-24, suggesting preferential expression of this gene in other tissues.

Whole-mount in situ hybridization (WISH) experiments were performed using anti-sense probes, which hybridize to native mRNA strands, from MEG-24 and MEG-27 to determine their expression loci in adult worms. The WISH assays revealed that expression of MEG-27 is concentrated in the region corresponding to the posterior esophagus of the parasite (Figure 1A). The absence of such signal in the negative control using a nucleotide probe corresponding to the sense RNA strand provides evidence of specific binding (Figure 1B). In contrast, MEG-24 does not exhibit any staining at the parasite esophagus, but displays a staining typical of proteins being expressed in subtegumental cells (Figure 1C), while no signal is noted in the negative control (Figure 1D).

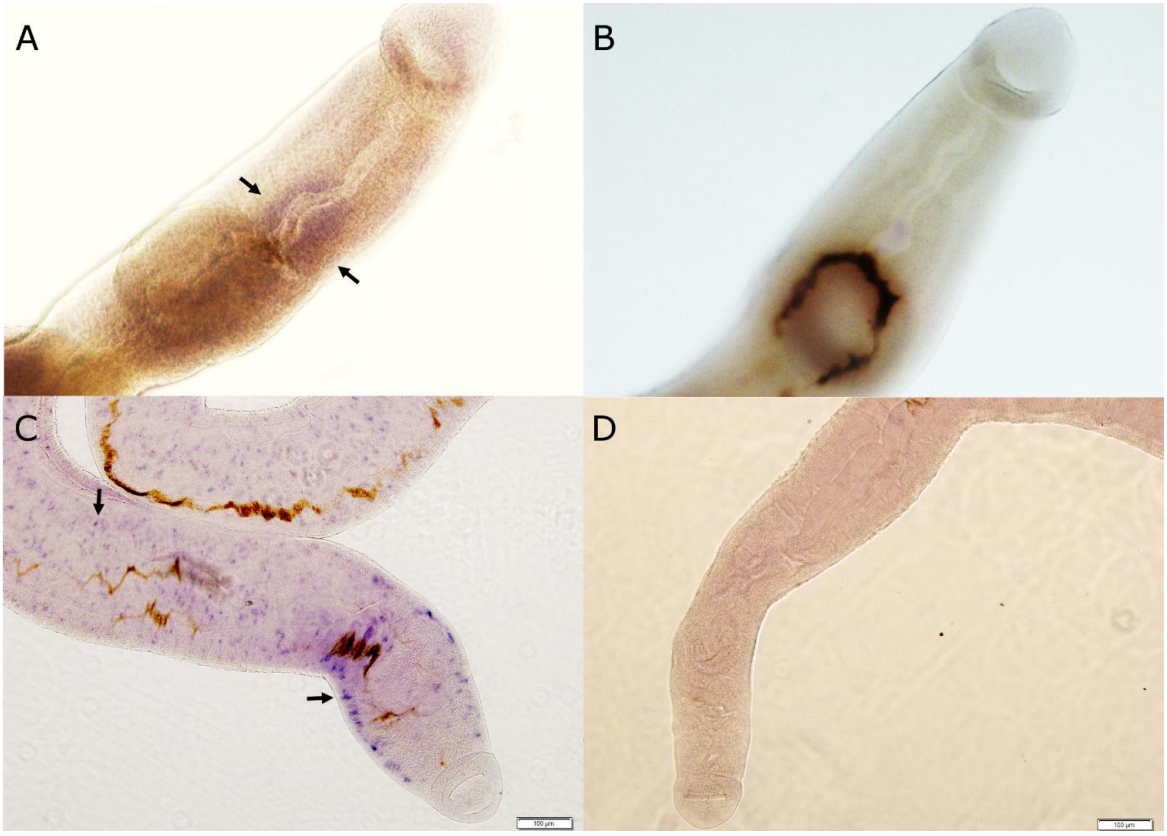

Figure 1. Differential localization of MEGs 24 and 27 in adult worm. (A) WISH using MEG-27 antisense probe revealing mRNA expression at the anterior esophagus gland. **(B)** Negative control incubated with MEG-27 sense RNA probe. **(C)** WISH using MEG-24 antisense probe showing labeling of subtegumental cells throughout the worm body. **(D)** MEG-24 sense probe, negative control.

3.2. MEG-24 and MEG-27 interact with mimetic membranes

The results from the WISH experiments support the hypothesis that both MEG-24 and MEG-27 act in different regions of the host parasite interface. It might be particularly interesting to investigate whether the properties of these proteins are similar to those of cationic α-helical membrane-active peptides. Therefore, lipid vesicles were employed to evaluate the effect of these peptides on the membrane structural integrity and to investigate how lipid environment may modulate the peptide structure.

MEG-27 and MEG-24 were incubated with POPC vesicles presenting different lipid compositions of cholesterol and sphingomyelin. Both proteins were able to promote the leakage of calcein from the zwitterionic POPC vesicles, indicating their ability to interact with

and disturb the packing of this model membrane (Figures 2A and 2B). At relatively high concentrations (5 mol% of peptide), approximately 80% leakage was observed for both proteins. The presence of either sphingomyelin or cholesterol in the POPC vesicles showed little effect on changing the lysis percentage of both MEG proteins, whereas the addition of POPG in the vesicle decreased the lytic effect caused by MEG-27 (Figure 2A). However, MEG-24 showed a distinct behavior depending on the concentration: below 1 mol%, a decreased lysis was also observed, whereas above 2 mol%, MEG-24 promoted higher permeabilization of POPG-containing LUVs (Figure 2B).

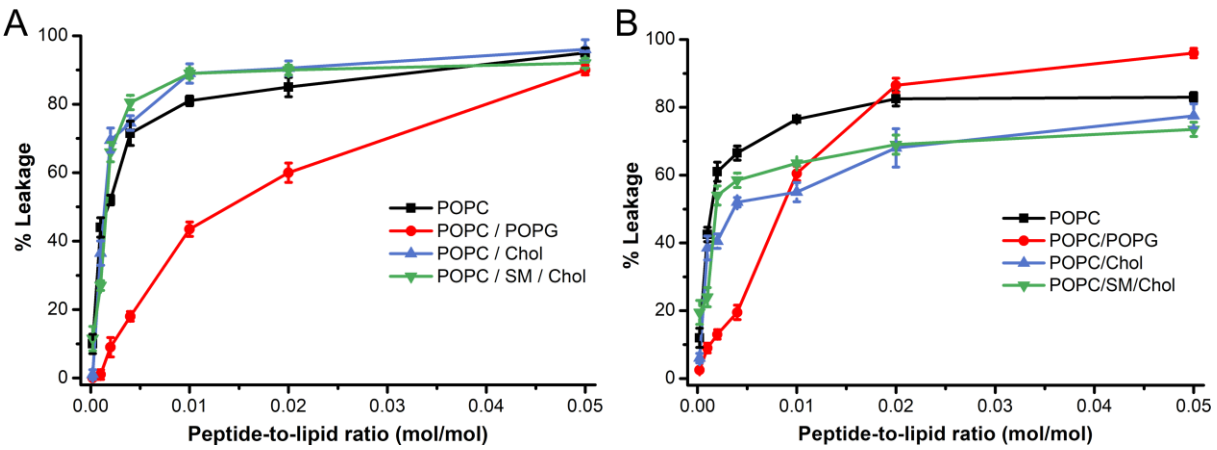

Figure 2. Permeabilization effect of MEG-27 and MEG-24 on lipid model membranes. Dose-response leakage data for **(A)** MEG-27 and **(B)** MEG-24 acting on POPC, POPC/POPG, POPC/Chol, and POPC/SM/Chol LUVs.

Since both MEGs presented high permeabilization activity on zwitterionic POPC vesicles, we carried out DSC experiments to better investigate the perturbation caused by the MEG proteins on the zwitterionic DMPC. DSC is a very sensitive technique for monitoring changes in the phase behavior of lipid membranes induced by external agents such as drugs [27], peptides , and proteins [29]. The calorimetric profile of DMPC large unilamellar vesicles exhibits two endothermic events related to membrane structural transitions: a less enthalpic and less cooperative pretransition at about 12 °C and a more energetic, very cooperative main

phase transition around 23 °C (black line in Figures 3A and B). The first transition corresponds to the formation of the ripple gel phase ($P_{\beta'}$), whereas the second transition arises from the conversion of $P_{\beta'}$ to the liquid crystalline phase (L_{α}). Both MEG-27 and MEG-24 change the thermotropic phase behavior of DMPC in a concentration-dependent manner (Figures 3A and B). MEG-27 perturbs both the pretransition and main phase transition more significantly than MEG-24. Indeed, the very narrow, cooperative peak at 24.0 ^{o}C in the protein-free DMPC LUVs becomes very broad in the presence of 2 mol% MEG-27 (linewidth increases from 0.6 ^{o}C to 8.1 ^{o}C), but is marginally affected by MEG-24 (0.87 ^{o}C) at the same concentration. This result indicates a more effective disruption of lipid-lipid interactions by the former MEG protein than by the latter. Furthermore, MEG-27 completely abolishes the DMPC pretransition, whereas vesicles with MEG-24 retains the lipid pretransition even at high concentrations (2 mol%). This suggests that MEG-27 interacts with DMPC membranes more superficially, at the headgroup level [29] whereas MEG-24 inserts into the lipid bilayer and does not significantly affect the headgroups. Taken together, our findings suggest different mechanisms of membrane disruption and, hence, lytic effect, induced by both MEG proteins. Based on effects previously described for antimicrobial peptides in membranes [30] , we hypothesize that the interaction of MEG-27 with DMPC disrupts the LUVs and putatively forms smaller vesicles, whereas MEG-24 binds to the membranes and possibly inserts among the lipid acyl chains, thus marginally perturbing the structural organization of the membrane.

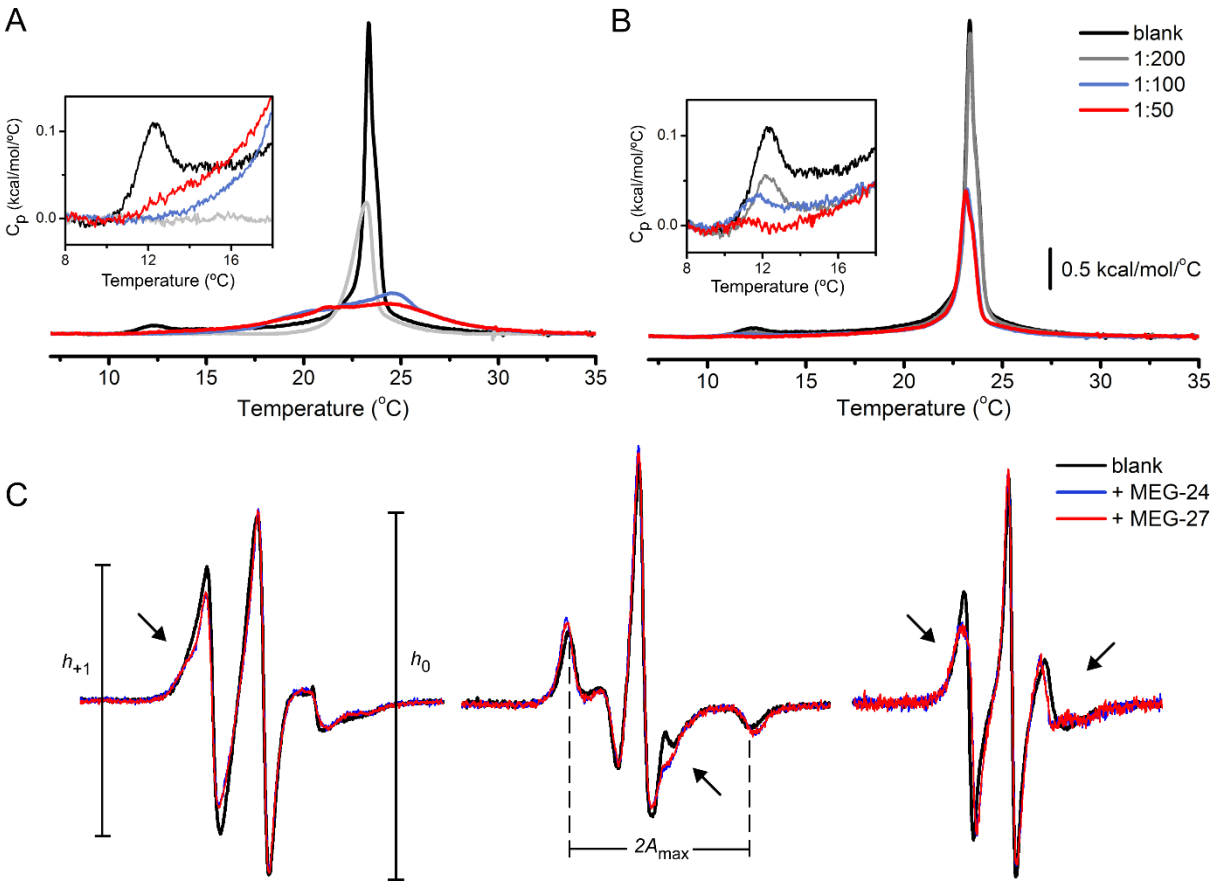

Figure 3. Effect of MEG-24 and MEG-27 on zwitterionic PC membranes. (A-B) Representative DSC profiles of DMPC LUVs without (black) and with **(A)** MEG-27 or **(B)** MEG-24 at different peptide-to-lipid molar ratios. The inset illustrates the effect of both proteins on the DMPC pretransition. **(C)** ESR spectra of DPPTC (left), 5-PCSL (center), and 16-PCSL (right) embedded in POPC SUVs in the absence (black) and presence of 3 mol% of MEG-24 (blue) and MEG-27 (red). The representative signals were acquired at 5 °C to highlight spectral differences induced by MEGs in the liquid crystalline phase of POPC. The arrows point to relevant line shape changes of the ESR spectra due to peptide binding. The empirical parameters h_{+1} and h_0 represent the height of the low- and middle-field resonance lines and $2A_{max}$ corresponds to the out-peak separation of the 5-PCSL spectrum. Scan range: 120 G for DPPTC and 5-PCSL, and 100 G for 16-PCSL.

Next, we sought to investigate in more details the degree of bilayer perturbation induced by both MEGs. To that end, we performed ESR experiments using spin-labeled lipids embedded into POPC small unilamellar vesicles to monitor changes on the lipid ordering and acyl chain mobility of the lipid bilayers upon addition of 3 mol% of the peptides, which correspond to the peptide concentration that promoted the highest lytic effect on a zwitterionic PC membrane − about 80% leakage in POPC (Figures 2A and B). ESR spectroscopy along

with spin labeling has been used to characterize the structural dynamics of both proteins and lipids in protein-membrane systems [31,32]. The use of phospholipids with nitroxide probes attached to different positions of the lipid acyl chain (5-PCSL and 16-PCSL) and the head group region (DPPTC) allowed reporting changes on the hydrophobic core of the membrane and at the membrane-water interface, respectively.

Addition of MEGs to POPC SUVs promotes dramatic changes on the ESR spectra of DPPTC, 5-PCSL, and 16-PCSL (Figure 3C). Both peptides profoundly alter the spectral line shape, causing line broadening to all signals. The reduction of the ratio of the amplitudes of the low- and central-field lines (h_{+1}/h_0) of both the DPPTC and 16-PCSL ESR spectra and the increase of the outer hyperfine splitting ($2A_{max}$) of the 5-PCSL spectrum qualitatively indicate an increase of the bilayer packing and/or a decrease of the membrane fluidity by the MEG proteins. Nonlinear least squares (NLLS) simulations of the ESR spectra were performed to quantitatively determine the contributions from both the rotational diffusion rate ($R_\perp$), which is an indicator of the membrane fluidity, and the order parameter (S_0), which is indicative of bilayer packing, of the spin-labeled lipids in POPC membranes.

NLLS spectral fitting (Figure S2) shows that both $R_\perp$ and S_0 are remarkably altered by MEG-24 and MEG-27, indicating that both lipid mobility and lateral ordering are perturbed (Supplementary Table S2). Indeed, $R_\perp$ decreased by approximately 30-35% for 5-PCSL and by about 9% for 16-PCSL in the presence of the proteins at 5 ^{o}C, a temperature at which spectral differences are more pronounced. The peptides also promote significant lipid lateral ordering of the POPC membrane, increasing the order parameter by 0.06-0.08 for 5-PCSL and by 0.10 for 16-PCSL at 5 ^{o}C (Table S2). This ordering effect has been reported for other membrane-interacting peptides such as antimicrobial peptides [33,34], cell-penetrating peptides [35], and viral fusion peptides [21,36]. Even though both peptides may disrupt membranes through different mechanisms, as suggested by DSC, the final peptide/lipid membrane complex,

formed after membrane disruption and leakage, displays very similar membrane fluidity and bilayer packing properties, as seen by ESR.

Synchrotron radiation circular dichroism (SRCD) spectroscopy was used to investigate whether the secondary structures of the peptides were altered by the presence of lipid vesicles. The two negative peaks at 222 and 208 nm and the positive peak around 192 nm in the SRCD spectrum of MEG-27 in water (Figure 4A) are characteristic of a peptide adopting an α-helix conformation, which qualitatively agrees with the structural prediction from the bioinformatics analysis. In the presence of POPC vesicles, the intensity of those bands is enhanced. As the POPC-to-MEG-27 molar ratio increased, so did the peak intensities at 192 and 222 nm (Figure 4A), suggesting that the partition of the peptide into the POPC vesicles results in a higher helix content of MEG-27. Secondary structure content estimation from SRCD spectra confirmed that the percentage of α-helix increased from 33% in the apo form to 59% in the presence of POPC vesicles at a 200:1 lipid-to-peptide molar ratio, whereas the unordered structure decreased from 34% to 27% (Table 1). Disorder-to-order transitions in the presence of lipids is a common trend in membrane-active peptides [37,38].

The SRCD spectrum of MEG 24 is characteristic of a peptide rich in helical structures and its devonvolution showed 61% of helix content (Figure S3). The CD spectra of MEG-24 in the presence of the zwitterionic vesicles, however, are virtually the same as the spectrum acquired in solution, maintaining the lineshape characteristic of an α-helix-rich structure under both conditions (Figure 4B).

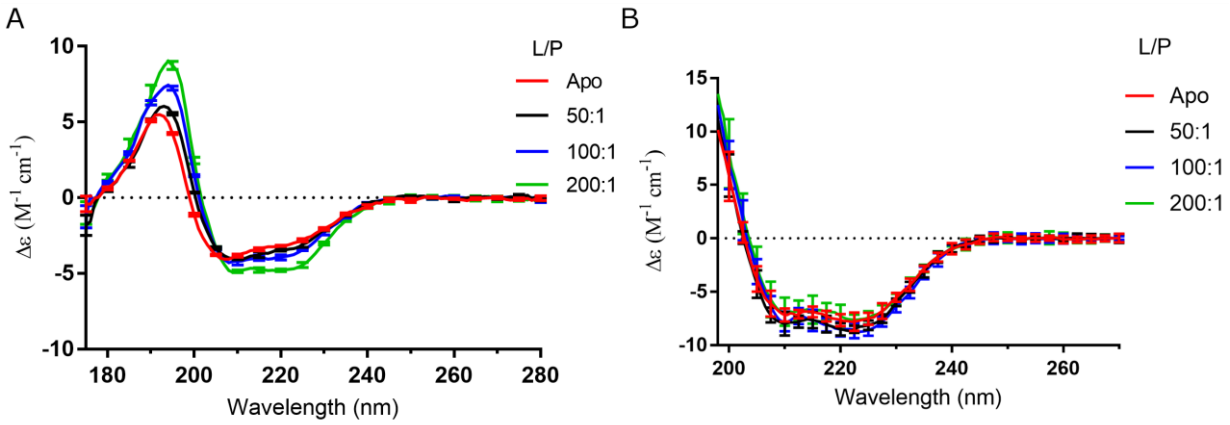

Figure 4. Circular dischroism spectra of MEG-27 and MEG-24 in POPC vesicles. (A) SRCD spectra of MEG-27 in water and in the presence of POPC vesicles at different lipid-to-peptide molar ratios (L/P). **(B)** CD spectra of MEG-24 in water and in the presence of POPC vesicles at different L/P.

Table 1: Deconvolution of SRCD spectra of MEG-27 in the apo form and in the presence of POPC vesicles at different lipid-to-peptide molar ratios.

	% helix	**% sheet**	**% turns**	**% unordered**	**NRMSD***
Apo	33	18	15	34	0.033
50:1	37	17	13	33	0.033
100:1	41	16	12	31	0.026
200:1	59	12	11	27	0.024

*NRMSD < 0.1 suggests the calculated spectra fit well to the experimental data.

MEG-27 has two tryptophan residues in its sequence; one of them is located within the hydrophobic face of the amphipathic helix (Figure S1), thus making it an excellent probe for interaction with membranes using intrinsic fluorescence measurements. When this peptide is incubated with POPC vesicles, a substantial blueshift from ~ 350 nm to ~ 330 nm is observed (Figure S4). Such a blueshift is characteristic of a decrease in solvent exposure and therefore indicates that one or both tryptophans are interacting with the vesicles [39,40]. MEG-24, on the other hand, does not have any Trp residues in its sequence to be monitored by fluorescence spectroscopy.

In aqueous solution, both peptides were able to migrate from the subphase to the water-air interface (Fig. 5A), presenting moderate surface activity throughout the time measured, causing surface pressure changes of 15 and 25 mN/m, respectively. MEG-27 presented higher surface activity compared to that of MEG-24, in agreement with the higher disturbing effect of MEG-27 in model membranes, previously seen by DSC. In addition, both MEG-24 and MEG-27 were able to adsorb onto the surface of POPC monolayers (Fig. 5B). The changes monitored in lateral pressure over time are due to the occurring peptide-lipid interactions at the monolayer surface. However, as the initial POPC lateral pressure was increased from 15 to 25 mN/m, the changes in lateral pressure were significantly reduced. Only a minor adsorption of MEG-27 onto the POPC monolayer with initial surface pressure of 35 mN/m was observed (surface pressure changes of ~4 mN/m). However, at this condition, no changes in lateral pressure have been detectec for the interaction with MEG-24.

The maximum insertion pressures (MIP) of MEG-24 in POPC monolayers was determined et ca. ~37 mN/m, suggesting its ability to disturb zwitterionic lipid systems, but preferably more fluid lipid system. Whereas for MEG-27, a MIP of ~43 mN/m was measured, which is well above the lateral pressure estimated for a biological membrane (30–35 mM/m) [41]and can be correlated to the observed efficiency of this peptide to disturb zwitterionic lipid systems.

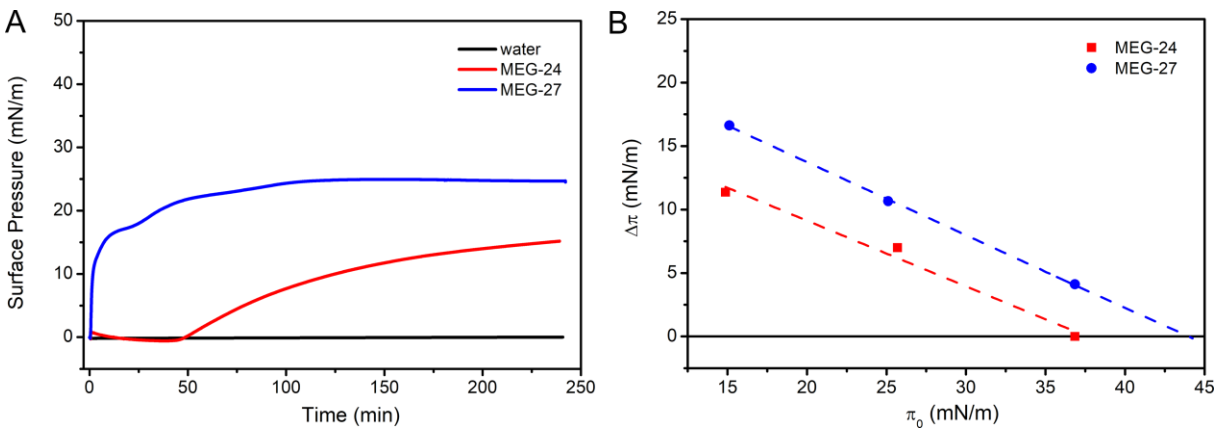

Figure 5. Surface properties of MEG-24 and MEG-27. (A) Surface activity of MEG-24 (red) and MEG-27 (blue) on an air–water interface. Black curve shows the surface pressure of an aqueous solution (control) throughout the assay. **(B)** Adsorption of MEGs (10 μM) onto POPC monolayers formed at the air–water interface under different initial surface pressures (π_0). Surface pressure changes ($\Delta\pi$) induced by peptide adsorption onto POPC monolayer were monitored.

3.3. MEG-24 is a pore-forming amphipathic helix

The helicoidal region of MEG-24 is predicted to have properties common to trans-spanning helices (Figure S1D) and the presence of a hydrophilic face in that helix suggests a pore-forming property for this peptide. To verify whether that was the case, the hemolytic activity of MEG-24 was tested. At a fixed concentration of 15 μM, about 20% of erythrocyte hemolysis occurred after one hour and a linear increase in hemolysis over time was observed, reaching 60% after 6 h of incubation (Figure 6A). From the concentration dependent experiment, a HC_{50} of approximately 40 μM was verified with 1 h incubation (Figure 6B), being considered a weakly hemolytic peptide [42] when compared to known efficient hemolytic peptides [43,44] It has been shown that incubating erythrocytes with polyethylene glycol (PEG) of different sizes allows efficient blockage of the pores induced by pore-forming peptides [45] . The effect of different PEGs on the hemolysis promoted by MEG-24 was tested and those exhibiting hydrodynamic diameters of at least 3 nm, such as PEG-3000, completely inhibited hemolysis (Figures 6C and 6D). This result indicates that the pores formed by MEG-24 display a cavity size of less than 3 nm. A similar pore size has been suggested for antimicrobial peptides like melittin [46] and defensins [43]. MEG-27 did not display hemolytic activity under the same conditions (data not shown).

In addition, the oriented CD spectrum of MEG-24 in planar POPC lipid bilayers shows a signal characteristic of a peptide inserted at a tilted angle (I-state) relative to the membrane surface (Figure S5), thus providing further evidence of a transmembrane topology [47]

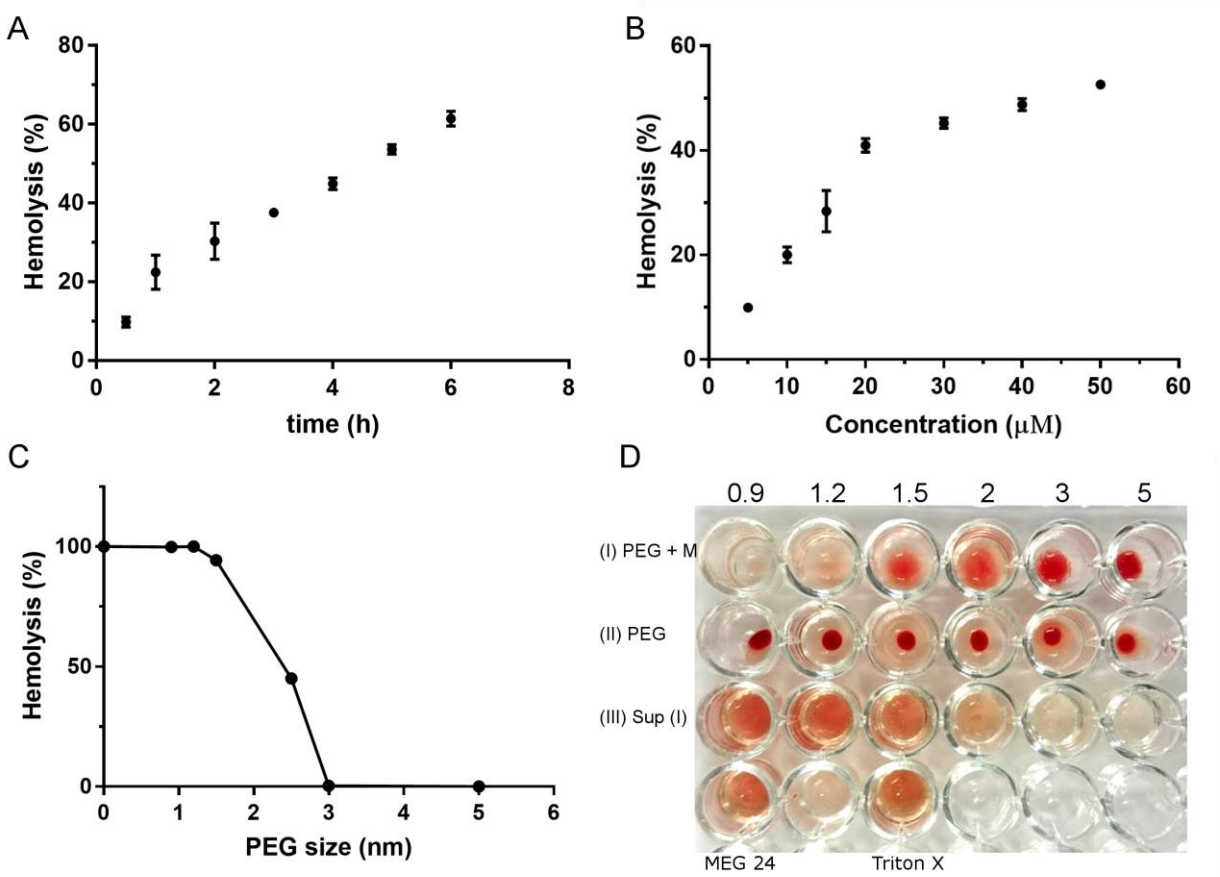

Figure 6. MEG-24 shows hemolytic activity. Hemolysis promoted by MEG-24 was monitored with increasing concentration of the peptide **(A)** or at a fixed concentration (15 μM) with increasing time **(B)**. **(C)** Hemolysis inhibition assay in the presence of PEGs of varied sizes. **(D)** Hemolysis and PEG inhibition assays as visualized in a 96-well plate (U bottom). Row I: erythrocytes in the presence of MEG-24 (80 μM) and different sized PEGs (0.9 − 5 nm). Row II: erythrocytes in the presence of PEGs only. Row III: supernatant of row I to better visualize the hemoglobin release. The last row shows the erythrocytes incubated with MEG-24 (80 μM) or TritonX-100 as the positive control of lysis.

3.4. MEG-24 and MEG-27 change the properties of cell membranes

To better understand the dynamics of the interaction of MEG-27 and MEG-24 with components of cellular membranes, DSC assays were performed on erythrocyte ghosts. The thermogram of the ghost erythrocyte membrane shows a very complex profile, in which four protein transitions can be observed (Figure 7A). The first peak, called transition I, refers to a domain formed by spectrin complexes; transition II corresponds to the denaturation of a domain formed by glycophorins and several proteins such as band 2.1, 4.1 and 4.2; the peak ascribed to III corresponds to the transition of the transmembrane protein domain of band 3,

and finally, transition IV has no clear description in the literature, being known only that they are due to proteins in the membrane [44].

The interaction of MEG-27 or MEG-24 with ghost erythrocyte membranes considerably alters the melting temperature of band 3 and changes the relative enthalpy, ΔH, between all transitions in a concentration-dependent manner (Figure 7A and 7B). The importance of band 3 protein has been ascribed to interactions with pathogens [48], hemoglobin [49], and the liberation of sphingosine 1-phosphate, which is associated with lymphocyte attraction [50], metabolic tissue sensor and a role in chloride shift [51] Therefore, changes in the band 3 protein may indicate an interesting mechanism for interaction, given the importance of this protein in several vital cellular processes. Interestingly, MEG-24 induced the formation of an additional peak at about 20 °C in the calorimetric profile of the ghost erythrocyte membrane in a concentration-dependent manner (Figure 7B). This transition vanishes upon denaturation of the erythrocyte ghost proteins, ruling out the possibility of being ascribed to particular lipid domains/structures induced by MEG-24. Therefore, this peak likely stems from the interaction between MEG-24 and ghost membrane proteins, but the real source is still unclear.

To gain further insights into the effects of the MEG proteins on the structural organization of the erythrocytes membranes, we performed ESR experiments using the spin-labeled lipids DPPTC, 5-PCSL, and 16-PCSL embedded into ghost erythrocyte membranes to monitor changes on the lipid ordering and mobility of distinct regions of the membranes.

Figures 7C and 7D illustrate representative ESR spectra of DPPTC, 5-PCSL, and 16-PCSL in erythrocyte ghost membranes at 37 ^{o}C in the absence and presence of 15 μM of MEG-27 (Figure 7C) and MEG-24 (Figure 7D). No alteration in the ESR lineshape was observed in the presence of 15 μM of MEG-24, a concentration that is known to promote 30% hemolysis of erythrocytes (Figure 5A) and to cause significant changes in the melting profile

of the ghost erythrocyte proteins (Figure 7B). This result suggests that the bulk lipids of the erythrocyte ghost membranes are not affected by MEG-24 binding.

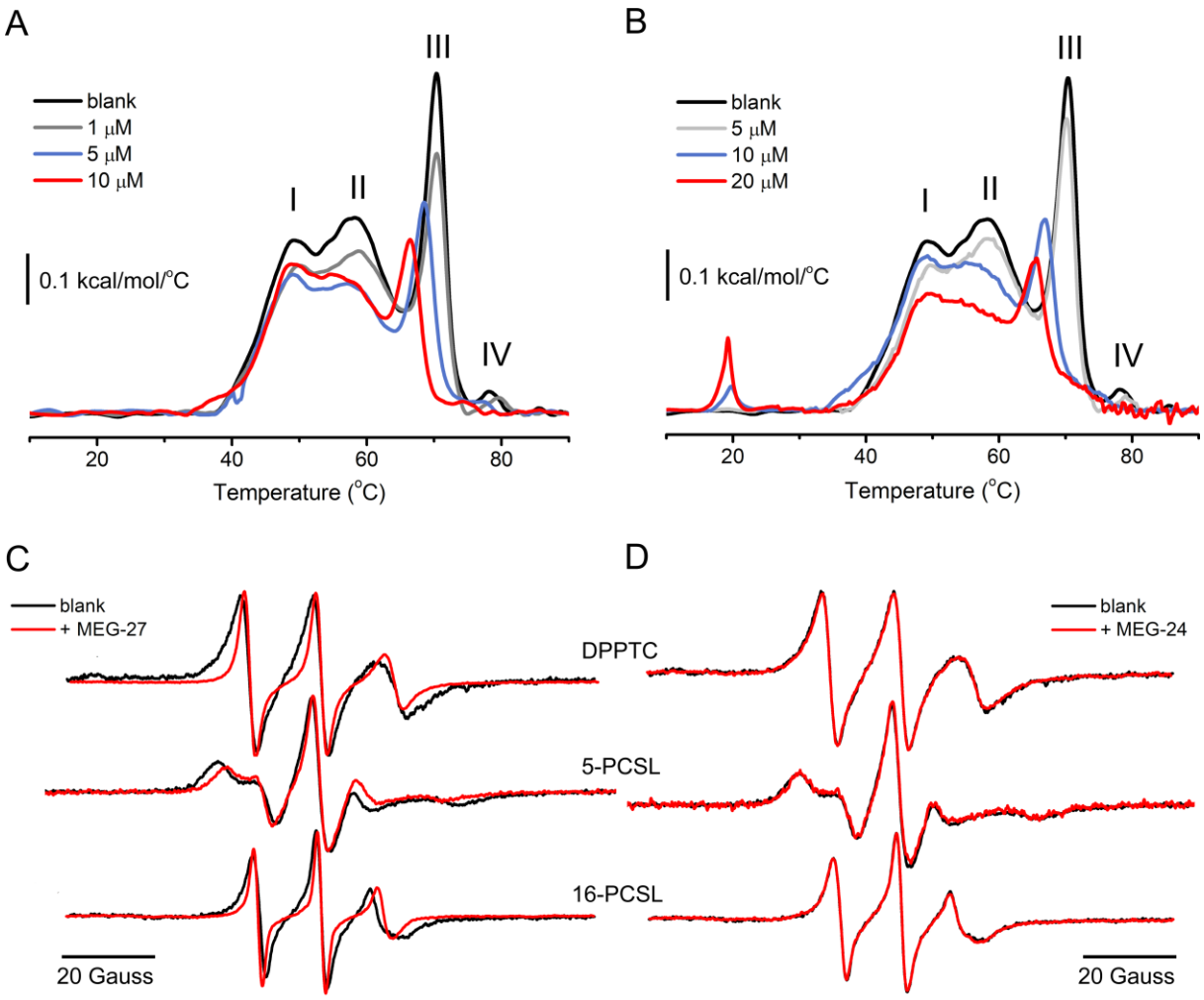

Figure 7. Effect of MEG-27 and MEG-24 on erythrocytes ghosts. (A-B) DSC thermograms of erythrocyte ghosts in the absence (black) and in the presence of **(A)** MEG-27 and **(B)** MEG-24 at different concentrations. **(C-D)** ESR spectra of DPPTC, 5-PCSL, and 16-PCSL embedded in the erythrocyte ghost membranes in the absence (black) and in the presence (red) of 15 μM of **(C)** MEG-27 and **(D)** MEG-24. Spectra were acquired at 37 ºC.

On the other hand, addition of MEG-27 alters the ESR line shape of all lipid probes, suggesting that this peptide has a large impact on membrane structure and dynamics that extends from the lipid/water interface down to the bilayer center. MEG-27 caused line narrowing of all spectra in a concentration-dependent manner (Figure S6). NLLS spectral

simulations suggest that both the mobility, $R_{\perp}$, and the ordering, S_0, of the spin-labeled lipids in the erythrocyte ghost membranes are significantly changed by the presence of MEG-27 (Figure S6 and Table S2). Indeed, $R_{\perp}$ increased by 58% (from 4.1 to 6.5 × 10^7 s^{-1}) for DPPTC, 37% (from 4.6 to 6.3 × 10^7 s^{-1}) for 5-PCSL, and 69% (2.3 to 3.9 ×10^8 s^{-1}) for 16-PCSL, whereas S_0 decreased by 0.25 for DPPTC, 0.09 for 5-PCSL, and 0.08 for 16-PCSL. These results show that MEG-27 promoted a pronounced fluidizing effect of the ghost erythrocyte membranes at high concentration (15 μM).

4. Discussion

The difficulty in assigning functions to MEG proteins derives from the lack of orthologs with described function. Moreover, MEGs were classified into families based on sequence homology, with no sequence similarity between members of different MEG families. However, most proteins coded by MEGs display very low molecular weight (< 10 kDa) and predictions of their secondary structures may offer hints as to their behaviors. An example of such approach was described for MEG-14, where bioinformatics analyses predicted an intrinsically disordered protein, which was later experimentally confirmed [7] and led to identification of a human interaction partner [8]. In the present work, two MEGs composed mostly of a cationic amphipathic helix displayed features similar to those described for α-helical membrane-active peptides, leading to their proposed interaction with biological membranes.

The MEGs coding for peptides with amphipathic helices clearly showed a tendency to interact with biological membranes. Both peptides interact with membrane mimetics leading to the leakage of entrapped calcein into vesicles. Moreover, peptide-lipid interactions promote an increase in MEG-27 α-helical content and alter the properties of DMPC vesicles and

erythrocytes ghosts, as assessed by DSC. Thus, we hypothesize that both MEG-24 and MEG-27 might play a role in the cell membranes or vesicular structures in the parasite.

Further analyses suggest that the dynamics of interaction of MEG-24 and MEG-27 with membranes are different. The hemolytic activity of MEG-24 and its inhibition by PEGs of specific sizes suggest that MEG-24 might act as a pore-forming peptide in complex cell membranes, such as red blood cells. MEG-24 also displays a small effect on the cooperativity of the melting transition and a marginal perturbation on the lipid headgroup, as seen by DSC. These results are consistent with the finding that MEG-24 acquires a tilted transmembrane topology, as shown by oriented CD. It has been shown that peptides displaying an amphipathic α-helix exhibit cell-penetrating properties, with formation of pores as a possible mechanism of their internalization [52] into mammalian cells. The low hemolytic activity by MEG-24 and its expression in the parasite tegument rather than in the esophagus, makes it unlikely that the role of MEG-24 is to promote hemolysis in a biological context.

MEG-27, however, affect lipid transitions and disturb lipid membranes more effectively than MEG-24. MEG-27 significantly perturbs the cooperativity of DMPC melting transition along with the pretransition, which is sensitive to changes in the headgroup structure. Even though MEG-27 does not promote hemolysis, it does perturb both proteins and lipids of ghost erythrocyte membranes. These results might suggest that MEG-27 causes membrane disruption by preferentially binding to the membrane surface. Particularly, a membrane surface adsorption could explain the remarkable changes of the ghost erythrocyte membrane fluidity measured by ESR. This contrasts with ESR results for the membrane-spanning MEG-24, where no change on the lipid fluidity and bilayer packing of the ghost membrane was observed. The lack of ESR spectral changes remains unclear to us, but it is tempting to speculate on that. The highest peptide concentration used in the ESR experiments with the ghosts is such that caused only 30% hemolysis of erythrocytes. Thus, at that

concentration, pore formation takes place with cavity size of up-to 3-nm diameter. Furthermore, the appearance of an additional peak on the DSC thermogram of the ghost erythrocyte/MEG-24 system in a concentration-dependent manner suggests the formation of a protein/peptide complex. MEG-24 does interact with ghost erythrocyte proteins and membrane. Therefore, the formation of local structures, such as pores or an erythrocyte protein/MEG-24 complex, are expected to have a reduced impact in the bulk lipids and may explain the lack of ESR spectral changes. We also do not discard the possibility of a cooperative effect of MEG-24 on the ghost erythrocyte membranes.

The findings observed for MEG-24 and MEG-27 in this study suggest that they are able to interact with both model and cell membranes through different mechanisms and can affect both lipid and proteins in more complex biological membranes in a manner simliar to that observed for several membrane-active peptides. It has been proposed that some membrane active peptides can play important roles in mammalian immune system [15, 49]. In fact, the analysis of the secretory proteome of the helminth *Fasciola hepatica* identified a 8 kDa protein with immune-modulatory properties which presented several features coincidental to MEG-24 and MEG-27, including the presence of a secretory signal peptide, prediction of an amphipathic helix and lack of conserved domain that could infer any known function [53,54]. Moreover, the cationic α-helical peptide LL-37 has been shown to be involved in modulation of inflammatory responses [55]. The interaction of MEG-14 with a human protein responsible for regulation of inflammatory responses has also been described [8]. Therefore, it is tempting to suggest that MEG-24 and MEG-27 may also interact with the host immune system, although experimental evidence is still lacking, which is a promising future direction in working with this intriguing class of MEG peptides with yet unknow function.

Acknowledgments

This work was funded by grants 2014/09361-9, 2015/50347-2 and 2018/19546-7 from the São Paulo Research Foundation (FAPESP). APF was recipient of a fellowship from CAPES. RDM, APUA, and JLSL are recipients of productivity fellowships from CNPq grants 304567/2017-5, 303229/2017-9, and 303513/2016-0, respectively. Funding to BAW was from grant P024092 and a UK-Brazil Partnership grant N012763, both from the UK Biotechnology and Biological Sciences Research Council (BBSRC). LGMB and AEZ thank FAPESP for the fellowship (Grant Numbers 2014/00206-0 and 2013/207154, respectively). PSK thanks CNPq for the fellowship grant #150417/2016-0. SRCD spectra were collected at AU-CD beamline at the ASTRID synchrotron (Denmark) under grants (to BAW, PSK and JLSL). The authors state no conflicts of interest.

Author Contributions

RDM and APUA conceived the study. APF, AEZ, LGMB, PSK, and JLSL performed the experiments. APF, AEZ, LGMB, PSK, JLSL, BAW, APUA, and RDM analyzed the data. APF, AEZ, LGMB, JLSL, BAW, APUA, and RDM wrote the manuscript.

References

[1] B. Gryseels, K. Polman, J. Clerinx, L. Kestens, Human schistosomiasis, Lancet. 368 (2006) 1106–1018.

[2] A.G.P. Ross, P.B. Bartley, A.C. Sleigh, G.R. Olds, Y. Li, G.M. Williams, D.P. McManus, Schistosomiasis, N. Engl. J. Med. 346 (2002) 1212–1220. doi:10.1056/NEJMra012396.

[3] M. Berriman, B.J. Haas, P.T. Loverde, R.A. Wilson, G.P. Dillon, G.C. Cerqueira, S.T.

Mashiyama, B. Al-lazikani, L.F. Andrade, P.D. Ashton, M.A. Aslett, D.C. Bartholomeu, G. Blandin, C.R. Caffrey, A. Coghlan, R. Coulson, T.A. Day, A. Delcher, R. Demarco, A. Djikeng, T. Eyre, J.A. Gamble, E. Ghedin, Y. Gu, C. Hertz-fowler, H. Hirai, Y. Hirai, R. Houston, A. Ivens, D.A. Johnston, D. Lacerda, C.D. Macedo, P. Mcveigh, Z. Ning, G. Oliveira, J.P. Overington, J. Parkhill, M. Pertea, R.J. Pierce, A. V Protasio, M.A. Quail, J. Rogers, M. Sajid, S.L. Salzberg, M. Stanke, A.R. Tivey, O. White, D.L. Williams, J. Wortman, W. Wu, M. Zamanian, A. Zerlotini, C.M. Fraser-liggett, B.G. Barrell, N.M. El-Sayed, The genome of the blood fluke Schistosoma mansoni, Nature. 460 (2009) 352–360. doi:10.1038/nature08160.

[4] R. DeMarco, W. Mathieson, S.J. Manuel, G.P. Dillon, R.S. Curwen, P.D. Ashton, A.C. Ivens, M. Berriman, S. Verjovski-Almeida, R.A. Wilson, Protein variation in blood-dwelling schistosome worms generated by differential splicing of micro-exon gene transcripts, Genome Res. 20 (2010) 1112–1121. doi:10.1101/gr.100099.109.

[5] G.S. Philippsen, R.A. Wilson, R. DeMarco, Accelerated Evolution of Schistosome Genes Coding for Proteins Located at the Host–Parasite Interface, Genome Biol. Evol. 7 (2015) 431–443. doi:10.1093/gbe/evu287.

[6] X.-H. Li, R. DeMarco, L.X. Neves, S.R. James, K. Newling, P.D. Ashton, J.-P. Cao, R.A. Wilson, W. Castro-Borges, Microexon gene transcriptional profiles and evolution provide insights into blood processing by the Schistosoma japonicum esophagus, PLoS Negl. Trop. Dis. 12 (2018) e0006235. doi:10.1371/journal.pntd.0006235.

[7] J.L.S. Lopes, D. Orcia, A.P.U. Araujo, R. DeMarco, B.A. Wallace, Folding Factors and Partners for the Intrinsically Disordered Protein Micro-Exon Gene 14 (MEG-14), Biophys. J. 104 (2013) 2512–2520. doi:10.1016/j.bpj.2013.03.063.

[8] D. Orcia, A.E. Zeraik, J.L.S. Lopes, J.N.A. Macedo, C.R. dos Santos, K.C. Oliveira, L. Anderson, B.A. Wallace, S. Verjovski-Almeida, A.P.U. Araujo, R. DeMarco,

Interaction of an esophageal MEG protein from schistosomes with a human S100 protein involved in inflammatory response, Biochim. Biophys. Acta - Gen. Subj. 1861 (2017) 3490–3497. doi:10.1016/j.bbagen.2016.09.015.

[9] R.A. Wilson, X.H. Li, S. Macdonald, L.X. Neves, J. Vitoriano-souza, L.C.C. Leite, L.P. Farias, S. James, D. Ashton, R. Demarco, W.C. Borges, The Schistosome Esophagus Is a ‘ Hotspot ’ for Microexon and Lysosomal Hydrolase Gene Expression : Implications for Blood Processing, PLoS Negl. Trop. Dis. 9 (2015) 1–25. doi:10.1371/journal.pntd.0004272.

[10] X. Li, W. De Castro-borges, S. Parker-manuel, G.M. Vance, R. Demarco, L.X. Neves, G.J.O. Evans, R.A. Wilson, The Schistosome Oesophageal Gland : Initiator of Blood Processing, PLoS Negl. Trop. Dis. 7 (2013) 1–15. doi:10.1371/journal.pntd.0002337.

[11] C.D. Fjell, J.A. Hiss, R.E.W. Hancock, G. Schneider, Designing antimicrobial peptides: form follows function, Nat. Rev. Drug Discov. 11 (2012) 37–51. doi:10.1038/nrd3591.

[12] M. Mahlapuu, J. Håkansson, L. Ringstad, C. Björn, Antimicrobial Peptides: An Emerging Category of Therapeutic Agents, Front. Cell. Infect. Microbiol. 6 (2016) 194. doi:10.3389/fcimb.2016.00194.

[13] H. Sato, J.B. Feix, Peptide–membrane interactions and mechanisms of membrane destruction by amphipathic α-helical antimicrobial peptides, Biochim. Biophys. Acta - Biomembr. 1758 (2006) 1245–1256. doi:10.1016/J.BBAMEM.2006.02.021.

[14] A.T.Y. Yeung, S.L. Gellatly, R.E.W. Hancock, Multifunctional cationic host defence peptides and their clinical applications, Cell. Mol. Life Sci. 68 (2011) 2161–2176. doi:10.1007/s00018-011-0710-x.

[15] Y. Lai, R.L. Gallo, AMPed up immunity: how antimicrobial peptides have multiple roles in immune defense., Trends Immunol. 30 (2009) 131–41.

doi:10.1016/j.it.2008.12.003.

[16] L. Käll, A. Krogh, E.L.. Sonnhammer, A Combined Transmembrane Topology and Signal Peptide Prediction Method, J. Mol. Biol. 338 (2004) 1027–1036. doi:10.1016/j.jmb.2004.03.016.

[17] E.L. Sonnhammer, G. von Heijne, A. Krogh, A hidden Markov model for predicting transmembrane helices in protein sequences., Proceedings. Int. Conf. Intell. Syst. Mol. Biol. 6 (1998) 175–82.

[18] A.A. Cogswell, J.J. Collins, P.A. Newmark, D.L. Williams, D.L. Williams, Whole mount in situ hybridization methodology for Schistosoma mansoni., Mol. Biochem. Parasitol. 178 (2011) 46–50. doi:10.1016/j.molbiopara.2011.03.001.

[19] C.W. McClare, An accurate and convenient organic phosphorus assay., Anal. Biochem. 39 (1971) 527–30.

[20] X. An, M. Salomao, X. Guo, W. Gratzer, N. Mohandas, Tropomyosin modulates erythrocyte membrane stability, Blood. 109 (2006) 1284–1288. doi:10.1182/blood-2006-07-036954.

[21] L.G.M. Basso, E.F. Vicente, E. Crusca, E.M. Cilli, A.J. Costa-Filho, SARS-CoV fusion peptides induce membrane surface ordering and curvature, Sci. Rep. 6 (2016) 37131. doi:10.1038/srep37131.

[22] A.J. Miles, B.A. Wallace, CDtoolX, a downloadable software package for processing and analyses of circular dichroism spectroscopic data, Protein Sci. 27 (2018) 1717–1722. doi:10.1002/pro.3474.

[23] L. Whitmore, B.A. Wallace, DICHROWEB, an online server for protein secondary structure analyses from circular dichroism spectroscopic data, Nucleic Acids Res. 32 (2004) W668–W673. doi:10.1093/nar/gkh371.

[24] J.G. Lees, A.J. Miles, F. Wien, B.A. Wallace, A reference database for circular

dichroism spectroscopy covering fold and secondary structure space, Bioinformatics. 22 (2006) 1955–1962. doi:10.1093/bioinformatics/btl327.

[25] L. Whitmore, B.A. Wallace, Protein secondary structure analyses from circular dichroism spectroscopy: Methods and reference databases, Biopolymers. 89 (2008) 392–400. doi:10.1002/bip.20853.

[26] E.N. Lorenzón, G.F. Cespedes, E.F. Vicente, L.G. Nogueira, T.M. Bauab, M.S. Castro, E.M. Cilli, Effects of dimerization on the structure and biological activity of antimicrobial peptide Ctx-Ha., Antimicrob. Agents Chemother. 56 (2012) 3004–10. doi:10.1128/AAC.06262-11.

[27] F.G. Avci, Membrane Active Peptides and Their Biophysical Characterization, 2017 (2018) 1–43. doi:10.3390/biom8030077.

[28] R.P. Barroso, L.G.M. Basso, A.J. Costa-Filho, Interactions of the antimalarial amodiaquine with lipid model membranes, Chem. Phys. Lipids. 186 (2015) 68–78. doi:10.1016/J.CHEMPHYSLIP.2014.12.003.

[29] E. Crusca, L.G.M. Basso, W.F. Altei, R. Marchetto, Biophysical characterization and antitumor activity of synthetic Pantinin peptides from scorpion's venom, Biochim. Biophys. Acta - Biomembr. 1860 (2018) 2155–2165. doi:10.1016/J.BBAMEM.2018.08.012.

[30] K.A. Brogden, Antimicrobial peptides: pore formers or metabolic inhibitors in bacteria?, Nat. Rev. Microbiol. 3 (2005) 238–50. doi:10.1038/nrmicro1098.

[31] L.G.M. Basso, L.F.S. Mendes, A.J. Costa-Filho, The two sides of a lipid-protein story, Biophys. Rev. 8 (2016) 179–191. doi:10.1007/s12551-016-0199-5.

[32] P.P. Borbat, A.J. Costa-Filho, K.A. Earle, J.K. Moscicki, J.H. Freed, Electron spin resonance in studies of membranes and proteins., Science. 291 (2001) 266–9. doi:10.1126/SCIENCE.291.5502.266.

[33] P. Kaur, Y. Li, J. Cai, L. Song, Selective Membrane Disruption Mechanism of an Antibacterial γ -AApeptide Defined by EPR Spectroscopy, Biophys. J. 110 (2016) 1789–1799. doi:10.1016/j.bpj.2016.02.038.

[34] J.H. Kleinschmidt, J.E. Mahaney, D.D. Thomas, D. Marsh, Interaction of bee venom melittin with zwitterionic and negatively charged phospholipid bilayers: a spin-label electron spin resonance study., Biophys. J. 72 (1997) 767–78. doi:10.1016/s0006-3495(97)78711-3.

[35] Z. Arsov, M. Nemec, M. Schara, H. Johansson, Ü. Langel, M. Zorko, Cholesterol prevents interaction of the cell-penetrating peptide transportan with model lipid membranes, J. Pept. Sci. 14 (2008) 1303–1308. doi:10.1002/psc.1062.

[36] M. Ge, J.H. Freed, Fusion Peptide from Influenza Hemagglutinin Increases Membrane Surface Order: An Electron-Spin Resonance Study, Biophys. J. 96 (2009) 4925–4934. doi:10.1016/j.bpj.2009.04.015.

[37] N.B. Last, D.E. Schlamadinger, A.D. Miranker, REVIEW A common landscape for membrane- active peptides, 22 (2013) 870–882. doi:10.1002/pro.2274.

[38] M. Sani, F. Separovic, How Membrane-Active Peptides Get into Lipid Membranes, (2016). doi:10.1021/acs.accounts.6b00074.

[39] K.M. Sanchez, J.E. Gable, D.E. Schlamadinger, J.E. Kim, Effects of tryptophan microenvironment, soluble domain, and vesicle size on the thermodynamics of membrane protein folding: lessons from the transmembrane protein OmpA., Biochemistry. 47 (2008) 12844–52. doi:10.1021/bi800860k.

[40] J.T. Vivian, P.R. Callis, Mechanisms of Tryptophan Fluorescence Shifts in Proteins, Biophys. J. 80 (2001) 2093–2109. doi:10.1016/S0006-3495(01)76183-8.

[41] D. Marsh, Lateral pressure in membranes., Biochim. Biophys. Acta. 1286 (1996) 183–223. doi:10.1016/s0304-4157(96)00009-3.

[42] O.S. Belokoneva, E. Villegas, G. Corzo, L. Dai, T. Nakajima, The hemolytic activity of six arachnid cationic peptides is affected by the phosphatidylcholine-to-sphingomyelin ratio in lipid bilayers, Biochim. Biophys. Acta - Biomembr. 1617 (2003) 22–30. doi:10.1016/J.BBAMEM.2003.08.010.

[43] W.C. Wimley, M.E. Selsted, S.H. White, Interactions between human defensins and lipid bilayers: evidence for formation of multimeric pores., Protein Sci. 3 (1994) 1362–73. doi:10.1002/pro.5560030902.

[44] A. Hernández-Hernández, M.C. Rodríguez, A. López-Revuelta, J.I. Sánchez-Gallego, V. Shnyrov, M. Llanillo, J. Sánchez-Yagüe, Alterations in erythrocyte membrane protein composition in advanced non-small cell lung cancer, Blood Cells, Mol. Dis. 36 (2006) 355–363. doi:10.1016/j.bcmd.2006.02.002.

[45] J. Smith, J. Manoranjan, M. Pan, A. Bohsali, J. Xu, J. Liu, K.L. McDonald, A. Szyk, N. LaRonde-LeBlanc, L.-Y. Gao, Evidence for Pore Formation in Host Cell Membranes by ESX-1-Secreted ESAT-6 and Its Role in Mycobacterium marinum Escape from the Vacuole, Infect. Immun. 76 (2008) 5478–5487. doi:10.1128/IAI.00614-08.

[46] K. Matsuzaki, S. Yoneyama, K. Miyajima, Pore Formation and Translocation of Melittin, 1997.

[47] J. Bürck, P. Wadhwani, S. Fanghänel, A.S. Ulrich, Oriented Circular Dichroism: A Method to Characterize Membrane-Active Peptides in Oriented Lipid Bilayers, Acc. Chem. Res. 49 (2016) 184–192. doi:10.1021/acs.accounts.5b00346.

[48] Q. Song, W. Song, W. Zhang, L. He, R. Fang, Y. Zhou, B. Shen, M. Hu, J. Zhao, Identification of erythrocyte membrane proteins interacting with Mycoplasma suis GAPDH and OSGEP, Res. Vet. Sci. 119 (2018) 85–90. doi:10.1016/J.RVSC.2018.05.001.

[49] A. Basu, A. Chakrabarti, Hemoglobin interacting proteins and implications of spectrin

hemoglobin interaction, J. Proteomics. 128 (2015) 469–475. doi:10.1016/j.jprot.2015.06.014.

[50] M. Kurano, M. Nishikawa, H. Kuma, M. Jona, Y. Yatomi, Involvement of Band3 in the efflux of sphingosine 1-phosphate from erythrocytes, PLoS One. 12 (2017) e0177543. doi:10.1371/journal.pone.0177543.

[51] N. Hamasaki, K. Okubo, Band 3 protein: physiology, function and structure., Cell. Mol. Biol. (Noisy-Le-Grand). 42 (1996) 1025–39.

[52] E. Koren, V.P. Torchilin, Cell-penetrating peptides: breaking through to the other side, Trends Mol. Med. 18 (2012) 385–393. doi:10.1016/j.molmed.2012.04.012.

[53] Y. Shai, Mechanism of the binding, insertion and destabilization of phospholipid bilayer membranes by alpha-helical antimicrobial and cell non-selective membrane-lytic peptides., Biochim. Biophys. Acta. 1462 (1999) 55–70.

[54] R.E. Hancock, G. Diamond, The role of cationic antimicrobial peptides in innate host defences., Trends Microbiol. 8 (2000) 402–10.

[55] J. Yu, N. Mookherjee, K. Wee, D.M.E. Bowdish, J. Pistolic, Y. Li, L. Rehaume, R.E.W. Hancock, Host defense peptide LL-37, in synergy with inflammatory mediator IL-1beta, augments immune responses by multiple pathways., J. Immunol. 179 (2007) 7684–91.

1.

Highlights

- MEG-24 and MEG-27 behave as the alpha helical antimicrobial peptides
- MEG-24
- MEG-27
- MEG proteins

Graphical Abstract

Picture?